



# Enhanced photocatalysis degradation of organophosphorus flame retardant using MIL-101(Fe)/persulfate: Effect of irradiation wavelength and real water matrixes



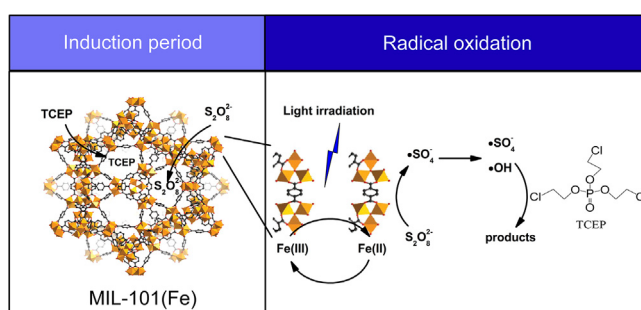
Han Hu, Haixuan Zhang, Ya Chen, Yujia Chen, Li Zhuang, Huase Ou\*

School of Environment, Guangdong Key Laboratory of Environmental Pollution and Health, Jinan University, Guangzhou 510632, China

## HIGHLIGHTS

- Powder MIL-101(Fe) is synthesized and has a bandgap at 2.41 eV.
- MIL-101(Fe)/420 nm/persulfate system has the highest degradation efficiency.
- Degradation of TCEP involves an induction period and a radical oxidation stage.
- Acid conditions are beneficial for the degradation using MIL-101(Fe).
- MOF/photo/persulfate system shows a robust performance in actual water matrixes.

## GRAPHICAL ABSTRACT



## ARTICLE INFO

### Keywords:

Persulfate  
Metal-organic framework  
Sulfate radical  
Natural water  
Water treatment

## ABSTRACT

Metal-organic-frameworks (MOFs) are novel classes of porous materials with diverse potentiality and easily tailored structures. Great challenges for the applications of MOF-based heterogeneous photocatalysis still exist, such as its stability and usability for real water bodies. In this study, MIL-101(Fe) was prepared and a MOF/photo/persulfate system was used to degrade tris(2-chloroethyl) phosphate (TCEP). Synthesized MIL-101(Fe) is high-purity regular crystal with a band gap energy at 2.41 eV, indicating that short wavelength visible light (400–520 nm) and ultraviolet light (200–400 nm) can be utilized by this MOF. Mechanism of photocatalysis reaction involved activation of MIL-101(Fe) for the transformation of Fe(III) to Fe(II), which induced further transformation of  $S_2O_8^{2-}$  to  $\cdot SO_4^-$ , and then TCEP was degraded by radical oxidation. The degradation pattern demonstrated a S-shape curve with two stages, induction period and radical oxidation. The former would be a process involving reactants adsorption and photocatalyst activation, while the later mainly included  $\cdot SO_4^-$  and/or  $\cdot OH$  reactions. Reaction rates of these two stages highly depended on activation wavelength and pH condition. Irradiation at 420 nm and acid condition were conducive to TCEP degradation, while high temperature and  $S_2O_8^{2-}$  addition accelerated the reaction. Five degradation products were elucidated, and the dominant degradation pathways included cleavage, hydroxylation, carbonylation and carboxylation. Furthermore, MIL-101(Fe)/420 nm/persulfate system demonstrated a more robust performance than homogeneous ultraviolet/persulfate system for TCEP removal in real water matrixes, implying that it will be a potential technology for elimination of organic pollutants in water.

\* Corresponding author.

E-mail address: [touhuase@jnu.edu.cn](mailto:touhuase@jnu.edu.cn) (H. Ou).

<https://doi.org/10.1016/j.cej.2019.02.190>

Received 17 November 2018; Received in revised form 23 February 2019; Accepted 25 February 2019

Available online 26 February 2019

1385-8947/ © 2019 Elsevier B.V. All rights reserved.

## 1. Introduction

Efficient elimination of trace organic chemicals (TOrc) from wastewater has become a hot research topic. Since traditional water treatment technologies can only partially remove TOrc, wastewater treatment plants (WWTPs) are considered as one of the most important sources and emitters of TOrc to environmental water bodies [1]. Recently, advanced oxidation processes (AOPs) have become prospective treatment methods for TOrc elimination. Familiar AOPs, such as ozonation ( $O_3$ ), ultraviolet(UV)-based AOPs ( $UV/H_2O_2$ ,  $UV/H_2O_2/O_3$ ,  $UV/H_2O_2/Cl^-$ , etc.), homogeneous Fenton ( $Fe^{2+}/H_2O_2$ ), have been well evaluated and applied in some full-scale water treatment facilities [2–4]. Some emerging AOPs, including electrochemical AOPs, plasma, cavitation based AOPs (ultrasonic), sulfate radical AOPs and photocatalytic AOPs, were also extensively studied [5–8]. Among these AOPs, sulfate radical AOPs (S-AOPs) can generate sulfate radicals ( $\cdot SO_4^-$ ) that possess a strong oxidation potential (2.6 V) under a wider pH range than hydroxyl radical ( $\cdot OH$ ) processes, meanwhile generate less disinfection by-products [9–12]. Heating, UV irradiation, homogeneous transition metal catalysis and heterogeneous photocatalysis are common activating method for S-AOPs [13,14]. For photocatalysis, a series of interfacial reactions between catalysts and oxidant donors (persulfate and peroxymonosulfate) generate highly reactive radical species, which can efficiently degrade refractory TOrc, e.g. pesticides [15], polycyclic aromatic hydrocarbons [16], antibiotics [17], etc.

Among the various metal catalysts, iron-based catalysts are attractive due to their affordability, biocompatibility and high activating efficiency [18]. Whereas, some weaknesses of iron catalysts still exist, such as reusability and minimise radical scavenging without diminishing reactivity [13]. Thus, it is desirable to develop novel iron-based catalysts to improve the performance of S-AOPs. Hybrid metal–organic frameworks (MOFs) are a class of the novel porous materials which have nearly infinite structures and magnificent features, such as high dispersibility, high surface area, semiconduction, microporosity and photosensitivity [19]. Typical MOFs are composed of metal-containing nodes connected by organic linkers through strong chemical bonds. Only some combinations are stable in water matrixes. For example, combinations of Ti, Zr, Fe, Al, Cr metals core nodes and carboxylate-based ligands were proven to be stable in acid and neutral water [20]. Among them, Fe-based MOFs may be highly practicable for photocatalysis due to their environment-friendly, low-cost and photo-responsive features.

Fe-based MOFs usually contain  $FeO_4(OH)_2$  octahedra or  $[Fe_3(\mu_3-O)(COO)_6]$  clusters secondary building units (SBUs) with carboxylate ligands, forming different topological structure series, such as MIL-53, MIL-100 and MIL-101 [20]. These SBUs commonly have trivalent iron ion (Fe(III)) metal nodes, and the electron transfer between the metal nodes and organic ligands will result in a variation from Fe(III) into Fe(II) (Eq. (1)), which can induce a transformation of oxidant donors to form reactive radicals (Eqs. (2) and (3)) [21]. Recently, researches testing these Fe-based MOFs as photocatalysts for organic pollutant degradation have only started. Some prototype MOFs, such as MIL-53(Fe) and MIL-88B(Fe), demonstrated better catalytic activities with  $H_2O_2$  than conventional catalysts ( $\alpha$ - $FeOOH$ ,  $Fe_2O_3$  and  $Fe_3O_4$ ) [22]. Combined with persulfate, MIL-53(Fe) also provided an accelerated photocatalytic degradation of dye [23]. Modified Fe-based MOFs were also developed to enhance their photocatalytic performance. Graphene oxide-MIL composite was synthesized, and its improving efficiency was attributed to the enhanced electron transport [24]. Cobalt and copper doped MIL-101(Fe) was made, and a higher persulfate activation efficiency was observed compared to original MIL-101(Fe), which may be due to alteration of morphology and structure [25]. Furthermore, to provide an recycling function, magnetic  $Fe_3O_4$  doped MOFs [26] and derived iron/carbon composites [27] were prepared. These exploratory research proved that Fe-based MOFs are versatile and will be potential photocatalysts to activate  $H_2O_2$ /

persulfate for organic pollutants elimination.



However, great challenges for the applications of Fe-based MOFs heterogeneous photocatalysis still exist due to the complexity of real water bodies. For example, most of the existing researches used dyes, which have high affinity to MOFs, but not actual organic pollutants as targets; Their degradation pathways and products were unclear. In addition, there is still a knowledge gap in regard to the optimization of activating wavelength and reaction conditions. To this end, tris(2-chloroethyl) phosphate (TCEP), an emerging organophosphorus ester in natural and industrial water bodies, was selected as the representative pollutant in this study. A tailor-made multiple wavelengths irradiation module, for the first time, was used to investigate the degradation efficiency of TCEP in a MIL-101(Fe)/photo/persulfate system. Degradation kinetics, mechanisms and products were determined, while the effects of anions and natural organic matter were explored. Furthermore, the performance of this system in artificial and real water matrixes was evaluated. This work can provide practicable information for the Fe-based MOFs photocatalysis of TOrc in water.

## 2. Materials and methods

### 2.1. Chemical reagents

TCEP (99%, HPLC grade) was obtained from Toronto Research Chemicals (CAN), while HPLC grade ethyl alcohol (EtOH), N, N-dimethylformamide (DMF), *tert*-butyl alcohol (TBA) and benzene-1,4-dicarboxylic acid ( $H_2BDC$ ) were acquired from Merck (Germany). Ascorbic acid (99%), formic acid (99.9%) and humic acid (HA) (90% dissolved organic matter, CAS: 1415–93-6) were purchased from Sigma-Aldrich (USA). Analytical grade  $Na_2S_2O_8$  (99%),  $FeCl_3 \cdot 6H_2O$  (98%),  $Na_2CO_3$  (98%), NaCl (98%),  $NaNO_3$  (98%) and  $Na_2SO_4$  (98%) were obtained from Sinopharm (China). HPLC grade acetonitrile and methanol were purchased from Fisher (USA). All reagents were used as received. All solutions were prepared using 18.2 M $\Omega$  ultrapure water or deionized water produced from a Milli-Q Advantage A10 system (Millipore, USA). Other chemical reagents were of the highest purity available.

### 2.2. Preparation and characterization of MOF

MIL-101(Fe) was prepared by a hydrothermal method based on the reported procedure with some modifications [28]. Typically, 1.351 g  $FeCl_3 \cdot 6H_2O$  (5 mmol) and 0.415 g (2.5 mmol)  $H_2BDC$  were mixed in DMF (30 mL), and then was sonicated for 20 min to make the solid fully suspension. The suspension was sealed into a Teflon-lined stainless steel autoclave and heated at 110 °C for 24 h. Orange mud was obtained and separated by centrifugation, and then it was washed by DMF and hot EtOH (60 °C, 3 h) for three times to remove the raw materials. The orange mud was dried at 70 °C for 60 min, and then activated at 150 °C for 12 h.

Characterization of MIL-101(Fe) includes its morphology, crystal structure, optical property and composition. First, morphology of MIL-101(Fe) was observed by a EVO18 scanning electron microscope (SEM) (Zeiss), while crystal structure and phase purity were determined by a D2 Phaser Desktop X-ray diffraction (XRD) (Bruker). A UV-3600Plus spectrophotometer (Shimadzu) with an integrating sphere was applied to characterize the UV–visible diffuse-reflectance spectrum (UV–VIS DRS), and its analyzed wavelength range covered 200–900 nm. A Nicolet iS50 infrared spectrometer (Thermo) was used to evaluate the

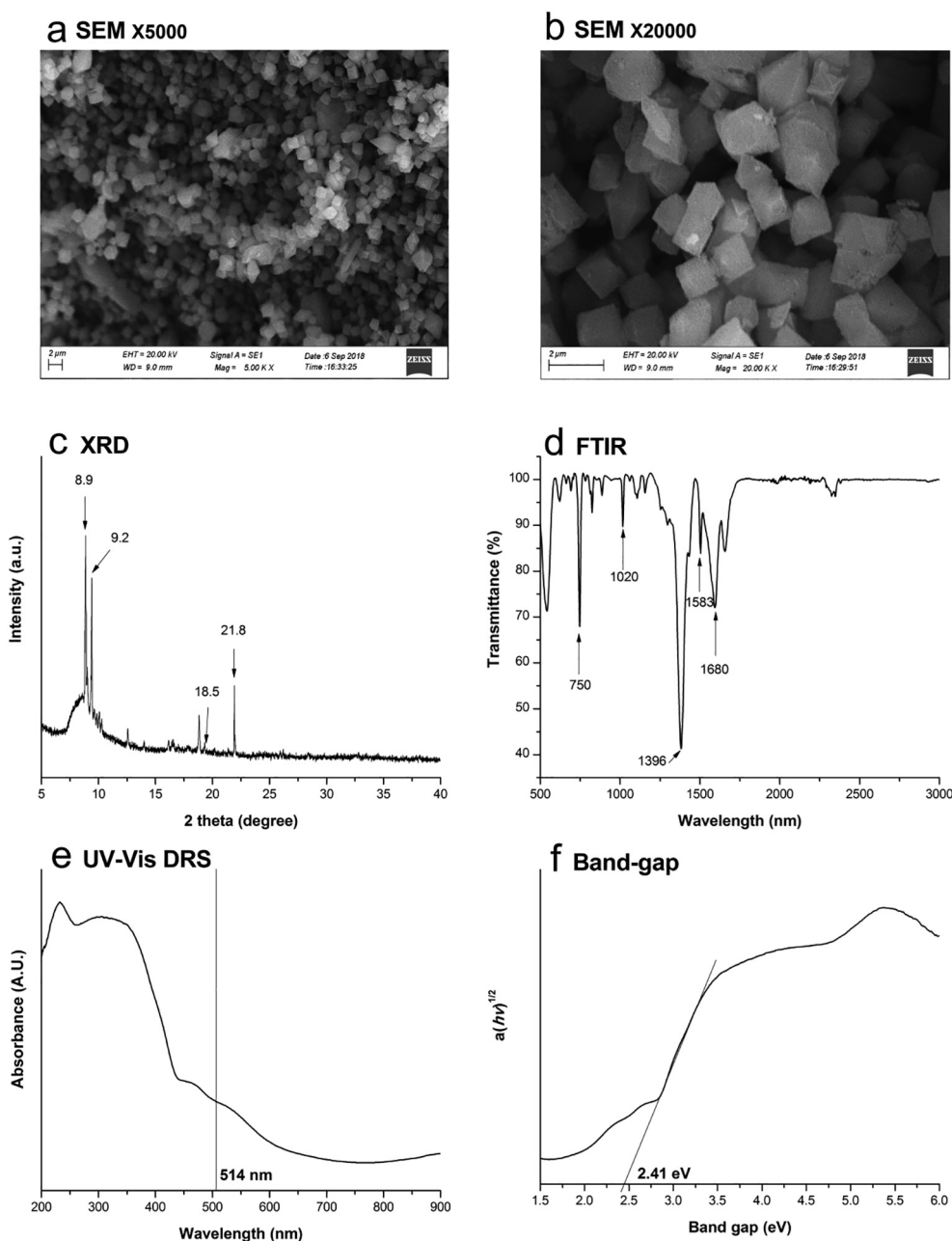


Fig. 1. Characterization of MIL-101 (Fe). (a-b) SEM images, (c) XRD spectrum, (d) FTIR spectrum, (e) UV-Vis DRS spectrum, (f) Band-gap energy.

Fourier transform infrared spectroscopy (FTIR), which reflected the composition and structure of MIL-101(Fe).

### 2.3. Basic photocatalysis experiments

A multiple wavelength irradiation module was made (Fig. S1), while it contained a light source, framework and reactor vessel. Light-emitting diodes (LEDs) with emission peaks at 280, 310, 365, 420, 472, 535, 587 and 625 nm were applied, and the irradiation intensity was measured using illuminometers. Visible light LEDs were purchased from NICHIA (Japan), and the power of a single LED is 3 W. UV-LEDs were obtained from OSRAM (Germany), and the power of a single UV LED is 0.1 W. A 6 × 6 UV-LED array was packaged and it has a power of ~3.6 W. The pH value of TCEP solution ( $[TCEP]_0 = 3.51 \mu\text{M}$ , 20 mL) was adjusted by buffered solution containing predefined concentration combinations of NaOH,  $\text{KH}_2\text{PO}_4$  and  $\text{H}_3\text{PO}_4$ , and then was transferred into the reactor vessel. The reaction solution was orbitally shaken at

60 rpm by a shaker and maintained at 288 K, 298 K and 308 K using magnetic stirrer with heating function. After adding given amount of solid MIL-101(Fe), a 30-min pre-adsorption was performed. Photocatalysis reactions began by adding given amount of  $\text{Na}_2\text{S}_2\text{O}_8$  stock solution and turning on the light sources with continuous shaking. At the pre-set times, 0.5 mL treated samples were obtained and filtrated by 0.22  $\mu\text{m}$  polyethersulfone filter. Reaction was stopped by adding equivalent ascorbic acid solution, and then transferred into brown amber tubes before analysis.

### 2.4. Influence factor, scavenging, recyclability and stability experiments

Influence factor experiments, included wavelength, pH, temperature, reactant ratio, anions and humic acid, were performed by adjusting solution conditions or adding specific reagents into the reaction system. To explore the reaction mechanism, scavenging experiment was performed. Only one scavenger (EtOH, TBA or ascorbic acid) at 100 mM

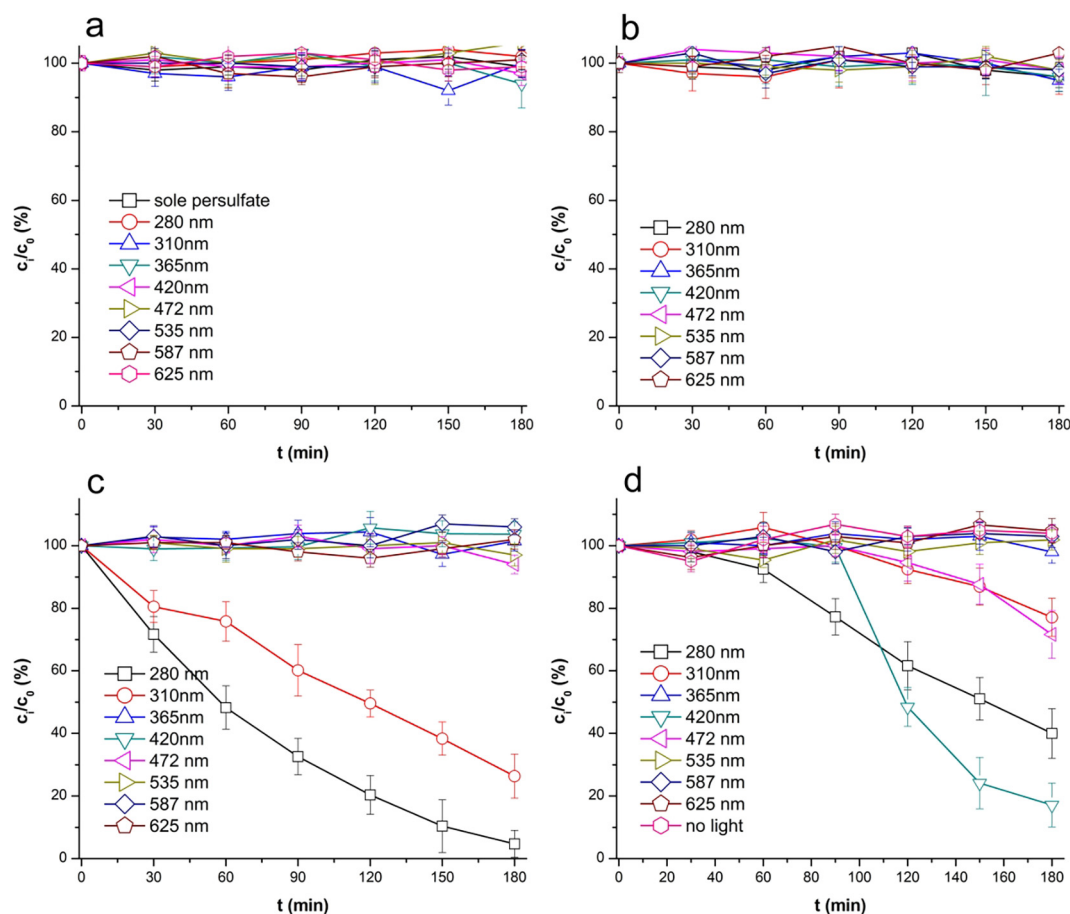


**Fig. 2.** Removal efficiencies of TCEP in MIL-101(Fe)/light/ $S_2O_8^{2-}$  system. (a) sole  $S_2O_8^{2-}$  and sole light irradiation, (b) light/MIL-101(Fe), (c) light/ $S_2O_8^{2-}$ , (d) MIL-101(Fe)/light/ $S_2O_8^{2-}$ , “no light” indicates MIL-101(Fe)/ $S_2O_8^{2-}$  system. Experimental conditions: normalized irradiation intensity =  $20.0 \text{ mW cm}^{-2}$ ,  $[TCEP]_0 = 3.51 \mu\text{M}$ ,  $[S_2O_8^{2-}]_0 = 500 \text{ mg L}^{-1}$ ,  $[MIL-101(Fe)]_m = 500 \text{ mg L}^{-1}$ , temperature =  $298 \text{ K}$ . All the experiments were carried out in triplicate with error bars representing the standard error of the mean.

was spiked into solution during one scavenging experiment. In recyclability experiment, suspension was centrifuged to separate the used powder after one reaction cycle, and then it was washed by 200 mL ultrapure water. After drying at  $60 \text{ }^\circ\text{C}$  for 10 h, a same amount of dried powder was used in the next batch of experiment under identical conditions. Total three cycles were applied. Analyses of dissolved ferric ion and ferrous ion concentrations using an iCAP RQ inductive coupled plasma emission spectrometer (Thermo Fisher) were conducted to evaluate the stability. Other reaction conditions were similar to Section 2.3.

### 2.5. Degradation of TCEP in real water matrix

Real water matrixes were collected from a drinking water treatment plant (DWTP) in Guangzhou City, China. The main treatment processes of this DWTP included pre-chlorination (chlorine dioxide), coagulation (poly aluminium chloride), sedimentation, filtration and disinfection (liquid chlorine). Source water (from Pearl River) and finished water (from DWTP) were obtained, and the analysis procedure of water parameters is presented in Text S2. Degradation experiment was conducted by adding pre-determined amounts of TCEP and MIL-101(Fe) into the real water matrix, and the main experimental procedure was similar to Section 2.3.

### 2.6. Determination of TCEP and degradation products

Determination of TCEP concentration was conducted using a HPLC/

MS<sup>2</sup> (TripleQuad 5500, AB-Sciex, USA). Determination of degradation products was performed using a TripleTOF 5600 + HRMS (AB-Sciex, USA). The product analysis procedure met the Level 3 in Schymanski Framework [29], thus, the identified products can be classified as tentative candidates. Detailed analysis process is presented in Text S1 and Tables S1.

## 3. Results and discussion

### 3.1. Characterization

SEM of MIL-101(Fe) is presented in Fig. 1a and 1b. MIL-101(Fe) was consisted of octahedron crystals at  $1.0\text{--}2.0 \mu\text{m}$  with smooth surface, which was similar to the previous researches [30,31]. XRD was used to identify the crystalline phase of MIL-101(Fe) (Fig. 1c). Peaks located at  $2\theta = 8.9^\circ, 9.2^\circ, 18.5^\circ$  and  $21.8^\circ$  were observed, which was resembled with the existing researches [32,33]. This indicated that the synthesized powder is high purity crystal. FTIR spectroscopy is displayed in Fig. 1d, with absorption peaks at around 750, 1020, 1396, 1583 and  $1680 \text{ cm}^{-1}$ . These characteristic peaks were consistent with reported MIL-101(Fe) [33]. Peak at  $750 \text{ cm}^{-1}$  indicates the C–H bending vibrations in benzene. Peaks at 1396 and  $1583 \text{ cm}^{-1}$  are assigned to symmetric and asymmetric vibrations of carboxyl groups (–COO–), respectively, while peak at  $1680 \text{ cm}^{-1}$  is related to C=O bonds in free carboxylic groups, indicating the dicarboxylate linker. These FTIR peaks represent the organic carboxylate bridging ligand structure. In short, these characterizations confirm that the orange powder is crystal

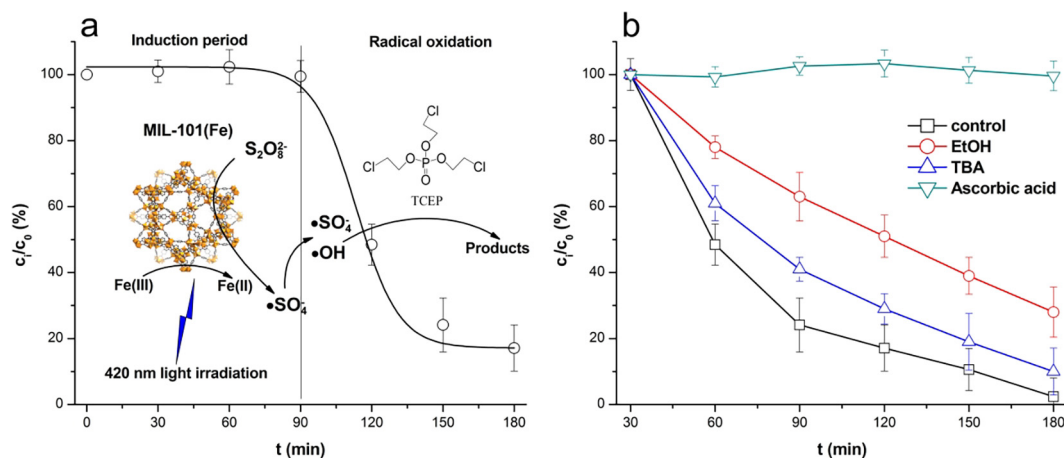


**Fig. 3.** Photocatalysis mechanism. (a) fitting curve and mechanism of reaction, (b) removal efficiencies in scavenger experiments. Experimental conditions: irradiation wavelength = 420 nm, irradiation intensity = 20.0 mW cm<sup>-2</sup>, [TCEP]<sub>0</sub> = 3.51 μM, [S<sub>2</sub>O<sub>8</sub><sup>2-</sup>]<sub>0</sub> = 500 mg L<sup>-1</sup>, [MIL-101(Fe)]<sub>m</sub> = 500 mg L<sup>-1</sup>, temperature = 298 K. All the experiments were carried out in triplicate with error bars representing the standard error of the mean.

pure MIL-101(Fe).

UV-vis DRS was used to analyze the photology properties of the MIL-101(Fe) (Fig. 1e). In UV range (200–400 nm), MIL-101(Fe) presented a high adsorption. For short wavelength visible light (400–600 nm), a weaker absorption was observed. A very low absorption was observed in the range of 600–900 nm, with a minimum value at ~750 nm. This UV-vis DRS suggested that MIL-101(Fe) may have a high utilization of irradiation in the range of 200–600 nm. The band gap energy ( $E_g$ ) can be estimated from the intercept of the tangents to the plots of  $A(h\nu)^{1/2}$  vs. photon energy, as shown in Fig. 1f [34]. The calculated  $E_g$  value is 2.41 eV, suggesting that light irradiation at wavelength lower than ~520 nm can promote valence electrons to become conduction electrons in MIL-101(Fe). Considering that natural organic matter and anions in real water bodies have significant screening effects against UV light but not visible light, irradiation at short wavelength visible light (400–520 nm) may be practicable for MIL-101(Fe)-based photocatalysis in real water.

### 3.2. Control degradation experiments and irradiation wavelength

A series of control experiments were performed. First, a pre-adsorption (1 mg L<sup>-1</sup> TCEP with 0.5 g L<sup>-1</sup> MIL-101(Fe)) was conducted, and MIL-101(Fe) only absorbed partial TCEP (~20%) within 30 min (Fig. S2). Adsorption equilibrium was achieved in initial 20 min. Variation of TCEP in sole Na<sub>2</sub>S<sub>2</sub>O<sub>8</sub> addition and sole light irradiation are presented in Fig. 2a. It seemed that these two control systems had negligible removal of TCEP. Persulfate is stable in normal environment, and it cannot react with TCEP directly. Furthermore, TCEP has been proven to be persistent under sunlight or even UV irradiation [8].

For light/MOF system, there was still no degradation (Fig. 2b). Light irradiation can excite MIL-101(Fe) to a high-energy state, resulting in separation of electrons and holes. However, the intensity of LED light source was 20 mW cm<sup>-2</sup>, which was much lower than that of xenon lamp (> 10<sup>3</sup>–10<sup>4</sup> mW cm<sup>-2</sup>). Thus, the electron-hole separation was relatively weak when no oxidant donor existed, which cannot induce direct transformation of TCEP. To the contrary, continuous removal of TCEP was observed in some light/persulfate systems (Fig. 2c). For example, > 90% TCEP was degraded within 180 min in 280 nm/persulfate system. Irradiation at 310 nm seemed to induce a weaker degradation. As the light wavelength increased, the degradation efficiencies tended to be poorer. UV-C (200–280 nm) and UV-B (280–320 nm) induced cleavage of S<sub>2</sub>O<sub>8</sub><sup>2-</sup> to generate  $\cdot SO_4^-$ , resulting in gradual degradation of TCEP. UV-A (320–400 nm) or visible light cannot induce this process. In our previous study, UV-C/persulfate

system has been confirmed to degrade TCEP effectively in pure water solution [35].

Degradation of TCEP in MIL-101(Fe)/light/persulfate systems (for short, MOF/photo/persulfate) with different wavelengths are shown in Fig. 2d. Unified concentration of different wavelength light sources was adjusted to 20.0 mW cm<sup>-2</sup>. Performance of this system highly depended on the irradiation wavelength. In general, degradation efficiency decreased in the order of 420 > 280 > 310 > 472 nm, while the systems with other wavelengths had no degradation. Of note, two different shapes of evolution curves were observed under different wavelengths. The curves of 420 nm demonstrated a S-shape tendency, suggesting that this system required an activating process. Short wavelength visible light (420 nm and 472 nm) can activate MIL-101(Fe) to an excited state, which was consistent with its band gap at ~2.4 eV (~520 nm, Fig. 1f). Under this condition, increasing conduction electrons transfer in MIL-101(Fe) induced a splitting of S<sub>2</sub>O<sub>8</sub><sup>2-</sup> to generate  $\cdot SO_4^-$ . Considering that solar light on the earth surface covers a large range of wavelength from ~300 nm to ~800 nm, this result implied that solar light can also induce photocatalysis reaction in MOF/photo/persulfate system. For UV systems, the curves of 280 nm and 310 nm presented continuous degradation, implying different degradation mechanisms. The lower degradation efficiencies may be due to the absorption of UV irradiation by MIL-101(Fe), which weakened the UV-induced cleavage of S<sub>2</sub>O<sub>8</sub><sup>2-</sup>. Furthermore, background NaOH, KH<sub>2</sub>PO<sub>4</sub> and H<sub>3</sub>PO<sub>4</sub> somewhat absorbed UV irradiation, aggravating this inhibition. In general, MOF/photo/persulfate system using 420 nm had the highest efficiency, which was employed in the following studies.

### 3.3. Degradation kinetics and mechanism

Degradation of TCEP in MIL-101(Fe)/420 nm/persulfate system demonstrated a S-shape curve (Fig. 2d). The decline tendency of TCEP was consisted of two stages, a slow decreasing stage and a rapid decline stage (Fig. 3a). These two stages were divided at the knee point of the S-shape curve. In the former stage, a slow degradation was observed, which lasted ~90 min in the current system. This stage was also reported in other studies using Fe-based catalysts [36,37], which was defined as the induction period. A kinetics parameter, induction time  $t_1$ , was used to describe its duration. It was defined as time to the knee of the best fit S-shaped curve, and its calculation followed a similar procedure reported by Luo *et al.* [37]. The later stage demonstrated a rapid decrease of TCEP. Based on the kinetics fitting, this stage followed a pseudo-first-order kinetics with an apparent rate constant  $k_{obs}$ , implying

**Table 1**  
Induction time ( $t_1$ ) and kinetic rate ( $k_{\text{obs}}$ ) of pseudo-first-order kinetics after induction period under different conditions.

Reaction system	$t_1$ (min)	$k_{\text{obs}}$ ( $\text{min}^{-1}$ )
MIL-101 + $\text{S}_2\text{O}_8^{2-}$ + 420 nm (control)	91	0.021
pH = 5.00	117	0.019
pH = 7.00	–	–
pH = 9.00	–	–
pH = 11.00	–	–
T = 288 K	119	0.020
T = 308 K	62	0.021
$[\text{S}_2\text{O}_8^{2-}]_m : [\text{MIL-101}]_m = 1 : 10$	108	0.019
$[\text{S}_2\text{O}_8^{2-}]_m : [\text{MIL-101}]_m = 1 : 2$	102	0.018
$[\text{S}_2\text{O}_8^{2-}]_m : [\text{MIL-101}]_m = 1 : 1$ (control)	91	0.021
$[\text{S}_2\text{O}_8^{2-}]_m : [\text{MIL-101}]_m = 1 : 0.66$	58	0.019
$\text{Cl}^-$	93	0.014
$\text{SO}_4^{2-}$	92	0.021
$\text{NO}_3^-$	91	0.021
$\text{CO}_3^{2-}$	98	0.015
Humic acid	118	0.008

Experimental conditions of control group: normalized irradiation intensity =  $20.0 \text{ mW cm}^{-2}$ ,  $[\text{TCEP}]_0 = 3.51 \mu\text{M}$ ,  $[\text{S}_2\text{O}_8^{2-}]_0 = 500 \text{ mg L}^{-1}$ ,  $[\text{MIL-101(Fe)}]_m = 500 \text{ mg L}^{-1}$ , pH = 3.00, temperature = 298 K.

that radical oxidation may be the dominant mechanism. Calculated  $t_1$  and  $k_{\text{obs}}$  are presented in Table 1. Of note, only the MIL-101(Fe)/420 nm/persulfate system had this S-shape tendency.

The mechanism of induction period is not fully clear due to the complicated heterogeneous reactions. Some researchers proposed that this period was the time for surface activation of catalysts [38]. Activation of MIL-101(Fe) may involve the transformation from Fe(III) to Fe

(II), which is induced by the electron transfer between the metal nodes and organic ligands. In MIL-101(Fe)/420 nm/persulfate system, a full activation will consume a time period to transform enough Fe(II), maintaining the interaction with persulfate to generate  $\cdot\text{SO}_4^-$ . Besides the internal electrical transfer, the external reactant transport onto catalyst could also affect reaction processes. Some scholars suggested that induction period may be the time for reactants to adsorb onto the catalysts [37]. Since MIL-101(Fe) is a spatial porous network, full adsorption of persulfate onto MIL-101(Fe) crystals to assess Fe-clusters will take a while, which may also contribute to the induction period.

To confirm the dominant reaction mechanism in the later radical oxidation stage, three typical scavengers were spiked respectively. It was observed that these scavengers have no effect on the induction period (data not shown), thus, only the degradation efficiency in the later stage was investigated (Fig. 3b). After adding 10 mM ascorbic acid, no evident degradation of TCEP was observed. Ascorbic acid is a strong reductant, and it has high reaction rate with various radicals, such as  $\cdot\text{OH}$  (Table S2). Thus, this inhibition suggested that the degradation of TCEP would be an oxidation reaction. To confirm the existence of radicals, EtOH and TBA were applied. EtOH has high reaction rate constants with both  $\cdot\text{OH}$  ( $k = 1.9 \times 10^9 \text{ M}^{-1} \text{ s}^{-1}$ ) and  $\cdot\text{SO}_4^-$  ( $k = 1.6 \times 10^7 \text{ M}^{-1} \text{ s}^{-1}$ ), while TBA has a high constant with  $\cdot\text{OH}$  ( $k = 6.0 \times 10^8 \text{ M}^{-1} \text{ s}^{-1}$ ) but a lower constant with  $\cdot\text{SO}_4^-$  ( $k = 4.0 \times 10^5 \text{ M}^{-1} \text{ s}^{-1}$ ). Therefore, the efficiency difference between the systems using these two scavengers can verify the existence of  $\cdot\text{SO}_4^-$ . Expectedly, both of these two scavengers had significant inhibition on reaction efficiency, and the inhibition of EtOH was more serious than that of TBA, indicating the existence of  $\cdot\text{SO}_4^-$ . Thus, the later stage could be dominant by  $\cdot\text{SO}_4^-$  and/or  $\cdot\text{OH}$  oxidation.

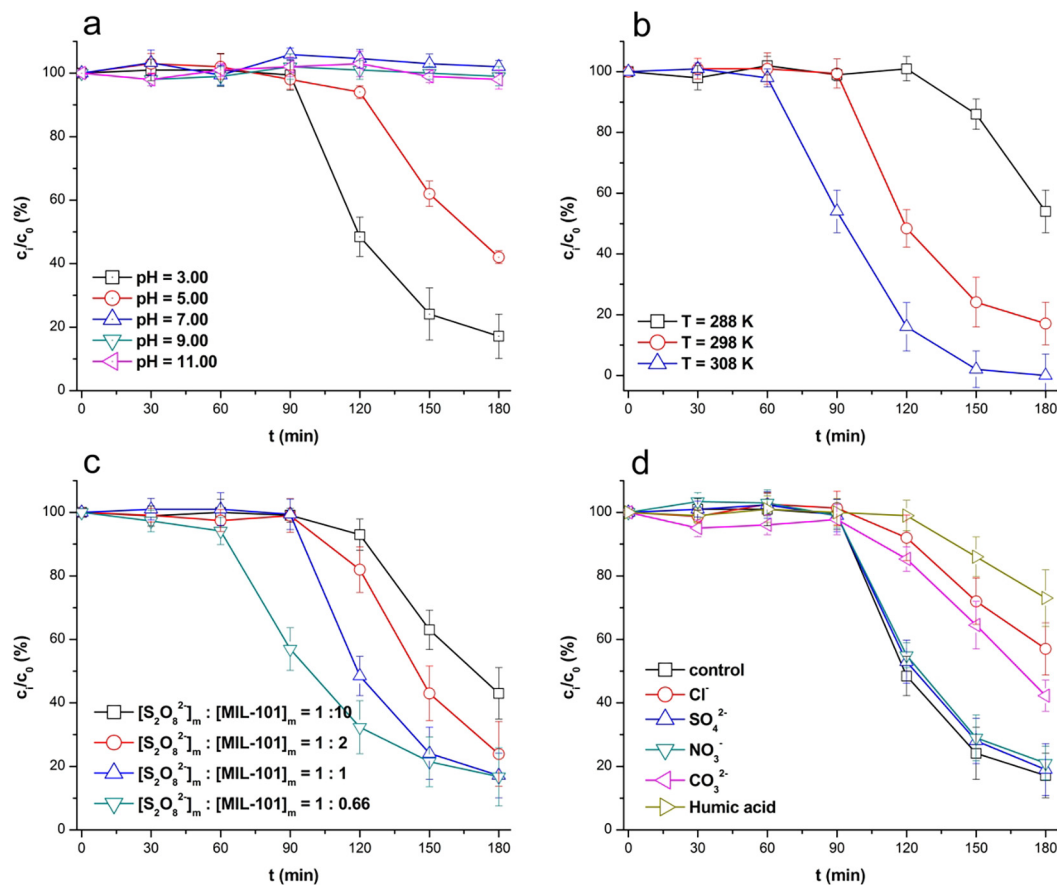


**Fig. 4.** Influence factors experiments. (a) effect of different pH values, (b) effect of temperature, (c) effect of  $[\text{MIL-101(Fe)}]_m : [\text{S}_2\text{O}_8^{2-}]_m$ ; (d) effect of anions and humic acid. Experimental conditions: irradiation wavelength = 420 nm, irradiation intensity =  $20.0 \text{ mW cm}^{-2}$ ,  $[\text{TCEP}]_0 = 3.51 \mu\text{M}$ ,  $[\text{S}_2\text{O}_8^{2-}]_0 = 500 \text{ mg L}^{-1}$ ,  $[\text{MIL-101(Fe)}]_m = 500 \text{ mg L}^{-1}$ , temperature = 298 K. All the experiments were carried out in triplicate with error bars representing the standard error of the mean.

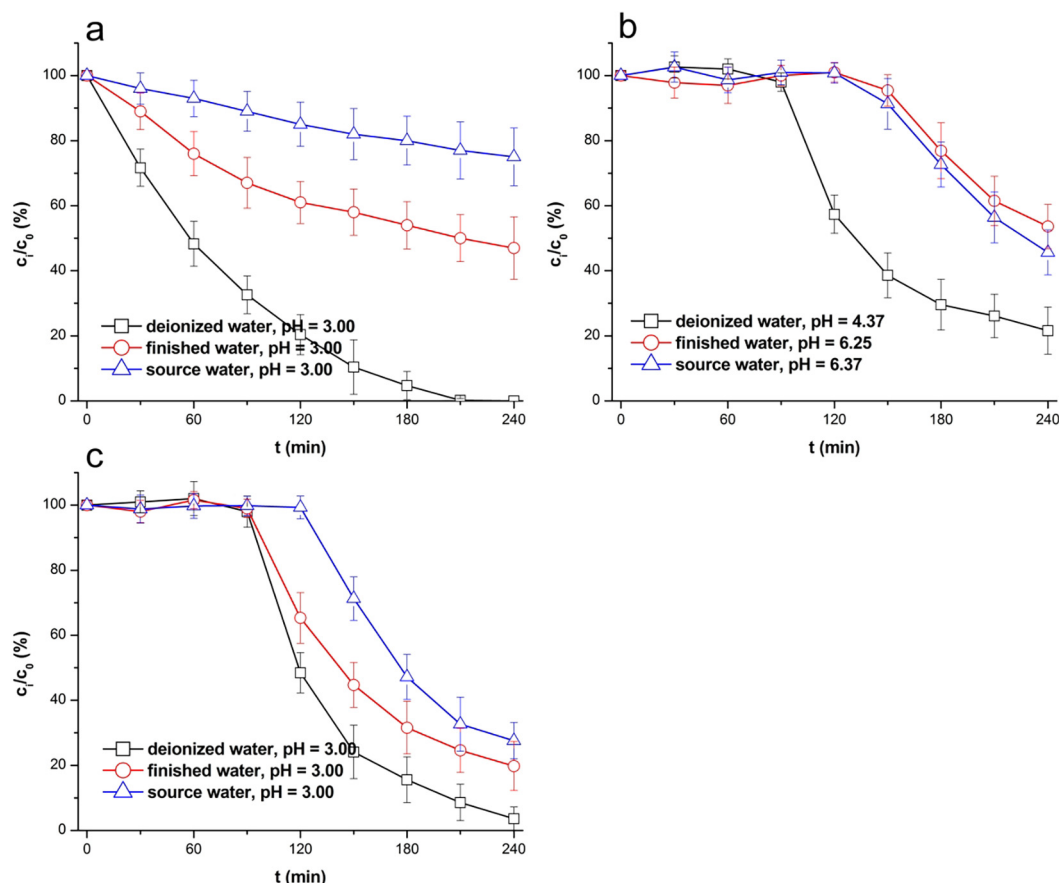


**Fig. 5.** Removal efficiencies of TCEP in actual water matrices. (a) homogeneous 280 nm/S<sub>2</sub>O<sub>8</sub><sup>2-</sup> system with pH adjustment (pH = 3.00), (b) 420 nm/MIL-101(Fe)/S<sub>2</sub>O<sub>8</sub><sup>2-</sup> system without pH adjustment, the pH value was obtained after adding MIL-101(Fe), (c) 420 nm/MIL-101(Fe)/S<sub>2</sub>O<sub>8</sub><sup>2-</sup> system with pH adjustment (pH = 3.00). Experimental conditions: irradiation intensity = 20.0 mW cm<sup>-2</sup>, [S<sub>2</sub>O<sub>8</sub><sup>2-</sup>]<sub>0</sub> = 500 mg L<sup>-1</sup>, [TCEP]<sub>0</sub> = 3.51 μM, [MIL-101(Fe)]<sub>m</sub> = 0.5 g L<sup>-1</sup>, temperature = 298 K. All the experiments were carried out in triplicate with error bars representing the standard error of the mean.

**Table 2**

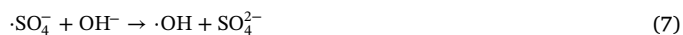
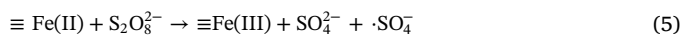
Induction time ( $t_1$ ) and kinetic rate ( $k_{obs}$ ) of pseudo-first-order kinetics after induction period in different actual water matrixes.

Reaction system	$t_1$ (min)	$k_{obs}$ (min <sup>-1</sup> )
S <sub>2</sub> O <sub>8</sub> <sup>2-</sup> + 280 nm		
deionized water, pH = 3.00	-	0.013
finished water, pH = 3.00	-	0.004
source water, pH = 3.00	-	0.001
MIL-101 + S <sub>2</sub> O <sub>8</sub> <sup>2-</sup> + 420 nm		
deionized water, pH = 4.37	96	0.013
finished water, pH = 6.25	146	0.006
source water, pH = 6.37	153	0.008
deionized water, pH = 3.00 (control)	91	0.021
finished water, pH = 3.00	99	0.018
source water, pH = 3.00	132	0.013

Experimental conditions of control group: normalized irradiation intensity = 20.0 mW cm<sup>-2</sup>, [TCEP]<sub>0</sub> = 3.51 μM, [S<sub>2</sub>O<sub>8</sub><sup>2-</sup>]<sub>0</sub> = 500 mg L<sup>-1</sup>, [MIL-101(Fe)]<sub>m</sub> = 500 mg L<sup>-1</sup>, temperature = 298 K.

On the basis of the results and discussions above, mechanism for TCEP degradation in MIL-101(Fe)/420 nm/persulfate system was supposed to involve two stages, induction period and radical oxidation stage (Fig. 3a). In the induction period, diffusion and adsorption of TCEP and persulfate onto MIL-101(Fe) crystals occurred. Furthermore, MIL-101(Fe) was excited by light irradiation to become a high-energy state. A charge separation and electron transfer from O<sup>2-</sup> to Fe(III) on the Fe-O clusters occurred, followed by the reduction of Fe(III) to Fe(II) (Eq. (4)). The accumulation of the above processes may be the dominant mechanisms of induction period, and it was the rate-determining

step during the whole reaction. In radical oxidation stage, the main reactions may include the interaction between Fe(II) and persulfate to generate extensive ·SO<sub>4</sub><sup>-</sup> and/or ·OH, while Fe(II) was oxidized to Fe(III) (Eqs. 5–7). Both ·SO<sub>4</sub><sup>-</sup> and ·OH can react with TCEP to generate a series of products (Eqs. (8) and (9)).



### 3.4. Influence factors

Based on the discussion in Section 3.3, changing the rate of internal electrical transfer and/or external reactant transport can alter the duration of induction period, while affecting the radical generation or quenching of radical itself can inhibit the radical oxidation. Thus, it is important to confirm the influence factors and determine their effects on this MOF/photo/persulfate system.

Influence factors experiments, including pH value, temperature, reactant ratio, anion and humic acid, were performed. First, pH had significant effects on degradation efficiency (Fig. 4a). The highest reaction rate was observed at pH 3.00, suggesting that acid condition was

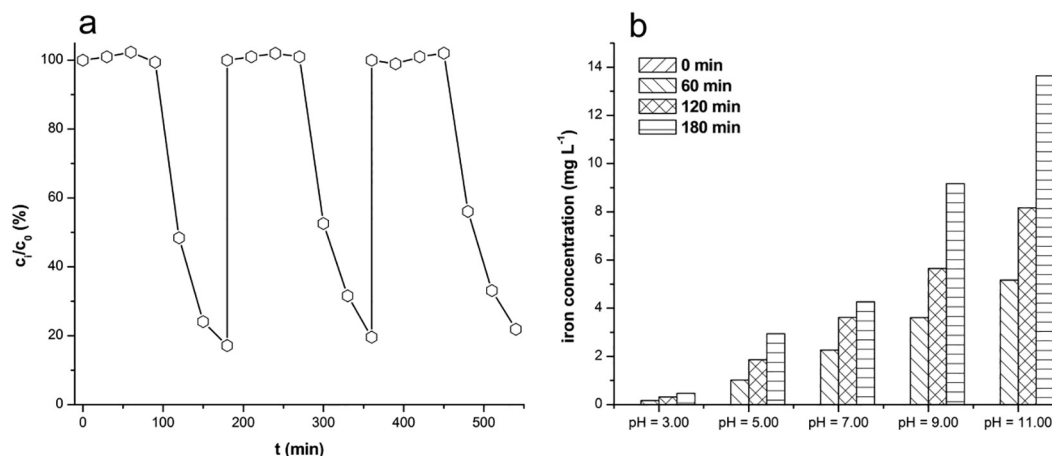
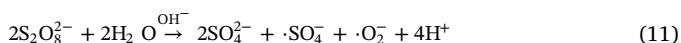


Fig. 6. Recyclability and stability. (a) recycling degradation performance, (b) iron concentration at different pH values. Experimental conditions: irradiation wavelength = 420 nm, irradiation intensity = 20.0 mW cm<sup>-2</sup>, [TCEP]<sub>0</sub> = 3.51 μM, [S<sub>2</sub>O<sub>8</sub><sup>2-</sup>]<sub>0</sub> = 500 mg L<sup>-1</sup>, [MIL-101(Fe)]<sub>m</sub> = 500 mg L<sup>-1</sup>, temperature = 298 K.

conductive to the MOF/photo/persulfate reaction. Both induction period and radical oxidation stage extended when pH increased. Under acid condition, more H<sup>+</sup> existed in the reaction system, while the protonation induced positive charged MIL-101(Fe). Thus, more S<sub>2</sub>O<sub>8</sub><sup>2-</sup> attracted onto MIL-101(Fe), resulting in a faster reactant transport and a shorter induction time. Under high temperature (e.g. 327 K or higher), H<sup>+</sup> will react with persulfate and form SO<sub>4</sub><sup>2-</sup> and ·SO<sub>4</sub><sup>-</sup> (Eq. (10)), which may weaken the degradation reaction [39]. However, this transformation may be negligible under ambient temperature (298 K) in the current experiments. Under basic condition, OH<sup>-</sup> can attach onto Fe(III) clusters, resulting in an inactivation of MIL-101(Fe). When pH further increased (pH > 12), the base (NaOH) was supposed to activate the persulfate into some other species, such as ·OH and ·O<sub>2</sub><sup>-</sup> [40] (Eq. (11)), which may improve the reaction efficiency. Here the pH value was in the range of 3–11, thus, the transformation of persulfate induced by base was also weak. Generally, effect of pH on the MIL-101(Fe) was the dominant one, and acid conditions were conducive to the MIL-101(Fe)/photo/persulfate reaction.



The second influence factor was temperature. As the temperature increased, a raising reaction efficiency was observed (Fig. 4b). For example, as temperature increased from 288 K to 308 K,  $t_1$  decreased from ~120 min to ~60 min, while  $k_{obs}$  maintained in the range of 0.020–0.021 min<sup>-1</sup>. The diffusions of TCEP and S<sub>2</sub>O<sub>8</sub><sup>2-</sup> were accelerated when temperature increased. Changing the [S<sub>2</sub>O<sub>8</sub><sup>2-</sup>]: [MIL-101(Fe)] ratio also affected the reaction efficiencies (Fig. 4c). When the S<sub>2</sub>O<sub>8</sub><sup>2-</sup> concentration increased, its probability to access MIL-101(Fe) also raised, which accelerated the external reactant transport. Effects of pH value, temperature, reactant ratio all supported the hypothetical mechanisms in Section 3.3.

Effect of different anions and humic acid are shown in Fig. 4d. Four anions had different effects on the reaction efficiency. As all anions and humic acid have little absorption against 420 nm irradiation, their inhibitions on reaction were mainly attributed to ·OH capture and/or catalyst inhibition. For example, SO<sub>4</sub><sup>2-</sup> and NO<sub>3</sub><sup>-</sup> have low reaction rate constants with ·OH (Table S2), and their inhibitions were negligible. To the contrary, both Cl<sup>-</sup> and CO<sub>3</sub><sup>2-</sup> have 10<sup>8</sup>–10<sup>9</sup> level reaction rate constants with ·OH. Thus, inhibition of degradation efficiency was observed in the presences these two anions. Humic acid is a common catalyst inhibitor, which can attach onto MIL-101(Fe) to reduce its active sites. Furthermore, it can react with ·OH, thus, its existence increased the  $t_1$  and decreased the  $k_{obs}$ . Of note, the concentration of these anions and humic acid was all 100 mg L<sup>-1</sup>, which was higher than their

common dosages in natural water bodies.

### 3.5. Degradation of TCEP in real water matrix

Two real water matrixes were used for the degradation of TCEP by MOF/photo/persulfate system. Basic parameters of water matrixes are presented in Table S3. Since the particulate materials in these matrixes were removed by 0.45 μm filters before reaction, their different effects on the reactions can be attributed to the dissolved impurities. Obviously, source water from the Pearl River contained more natural organic matter and anions than the finished water (Table S3). Homogeneous UV/persulfate systems were applied to compare the degradation performance (Fig. 5a). In the control system (280 nm/persulfate in deionized water), degradation of TCEP followed a fast procedure with  $k_{obs}$  at 0.013 min<sup>-1</sup> (Table 2). Whereas, the impurities in real waters had critical inhibition on reaction efficiency. For example,  $k_{obs}$  decreased to 0.004 min<sup>-1</sup> and 0.001 min<sup>-1</sup> in finished water and source water, respectively. It was well known that common contaminants in natural water bodies had significant screening of UV irradiation, which may be the reason.

However, it was not true for MOF/photo/persulfate system using visible light. Degradation efficiency in these systems differed from water sources and pH conditions. In the experiments without pH adjustment, the original pH values were around 7.0 in finished water and source water, while deionized water was 6.1. After adding 0.5 g L<sup>-1</sup> MIL-101(Fe), pH of finished water and source water reduced to 6.25 and 6.37. For the deionized water, pH reduced to 4.37. High pH value was not conducive to the MOF/photo/persulfate system, resulting in significant inhibition of degradation efficiencies without pH adjustment (Fig. 5b). In finished and source water systems, induction time  $t_1$  increased to 146 min and 153 min, while  $k_{obs}$  decreased to 0.006 min<sup>-1</sup> and 0.008 min<sup>-1</sup>.

After all the pH values were adjusted to 3.00, compared to deionized water (control group), two real water matrixes had slightly higher  $t_1$  and lower  $k_{obs}$  (Table 2). For example,  $t_1$  and  $k_{obs}$  were 91 min and 0.021 min<sup>-1</sup> in deionized water, while they were 99 min and 0.018 min<sup>-1</sup> in finished water. The slight inhibition can be attributed to the higher dosage impurities in these two real water matrixes than those in deionized water. For example, the TOC were 28.63 and 4.14 mg L<sup>-1</sup> in real waters, while it was 0.08 mg L<sup>-1</sup> in deionized water. Furthermore, high concentration anions were also observed in two real waters. According to the results in Section 3.4, all these impurities affected the reaction efficiency at pH 3. Since these common impurities have little absorption at 420 nm (OD<sub>420</sub> in Table S3), the dominant inhibition mechanism may be radical quenching but not light screening. Nonetheless, removal of TCEP reached 72% and 80% in raw

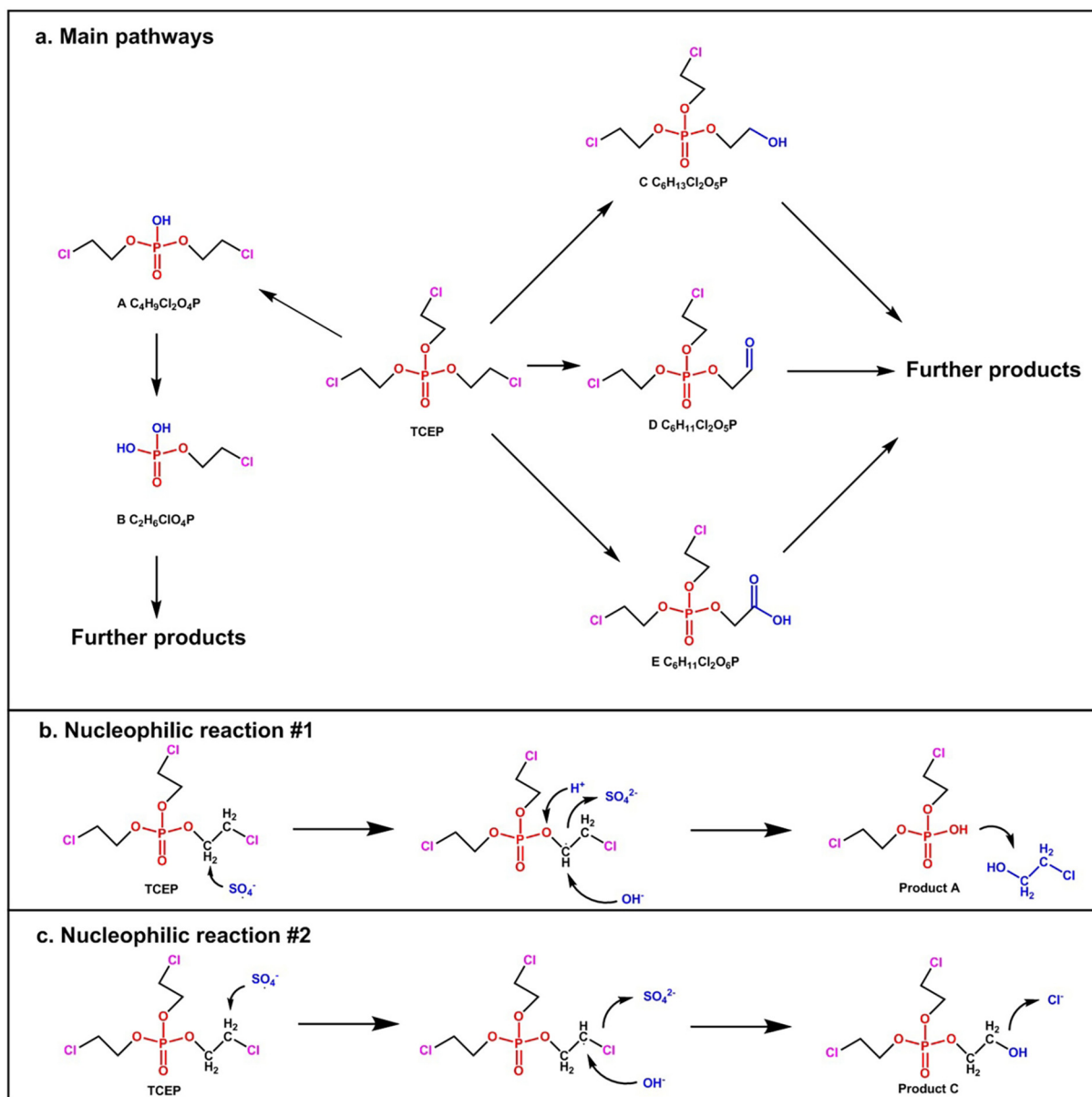


Fig. 7. Proposed generation pathways of TCEP degradation products. (a) main pathways, (b) nucleophilic reaction #1, (c) nucleophilic reaction #2. Experimental conditions: irradiation wavelength = 420 nm, irradiation intensity = 20.0 mW cm<sup>-2</sup>, [TCEP]<sub>0</sub> = 3.51 μM, [S<sub>2</sub>O<sub>8</sub><sup>2-</sup>]<sub>0</sub> = 500 mg L<sup>-1</sup>, [MIL-101(Fe)]<sub>m</sub> = 500 mg L<sup>-1</sup>, temperature = 298 K.

water and finished water, respectively, after 240-min MOF/photo/persulfate reaction, while the ones were 20% and 48% in homogeneous UV/persulfate. In general, this MOF/photo/persulfate system showed a more robust performance, especially after pH adjustment, for organic contaminants removal in real water matrixes. Considering that the pH is usually around 7 in real drinking water treatments, modifications of MIL-101(Fe) to extend its pH flexibility are desirable.

### 3.6. Electrical energy evaluation

Electrical energy of light irradiation was evaluated by electrical energy per order (EE/O), which is defined as the electrical energy (kWh) required to degrade a contaminant by an order of magnitude in 1 cm<sup>3</sup> matrix. Detailed calculation followed a similar procedure reported in our previous study [8]. Since two stages in MOF/photo/persulfate system both consumed light energy, their EE/O values were calculated respectively, while the total EE/O value was the sum of them. EE/O values in the reactions using different water matrixes are

presented in Table S4. In the control group (deionized water, irradiation intensity = 20.0 mW cm<sup>-2</sup>, [S<sub>2</sub>O<sub>8</sub><sup>2-</sup>]<sub>0</sub> = 500 mM, [TCEP]<sub>0</sub> = 3.51 μM, [MIL-101(Fe)]<sub>m</sub> = 0.5 g L<sup>-1</sup>, temperature = 298 K), the total EE/O value was 25.96 kWh m<sup>-3</sup> order<sup>-1</sup>. It increased as the induction time *t*<sub>1</sub> increased and the *k*<sub>obs</sub> decreased. When using real water without pH adjustment, the total EE/O increased to nearly twice as that in control group. After pH was adjusted to 3.00, total EE/O declined. All these EE/O values were significantly higher than those (usually at 10<sup>-2</sup>–10<sup>-1</sup> level) in UV-based radical oxidation system for TCEP degradation [8,41]. Since the applied irradiation intensity at 20.0 mW cm<sup>-2</sup> was much lower than that of sunlight on earth surface, if using sunlight as light source for this MOF/photo/persulfate system, a higher degradation efficiency may be achieved, and this energy consumption may not be an obstacle.

### 3.7. Recyclability and stability

Recyclability is crucial for applications of heterogeneous

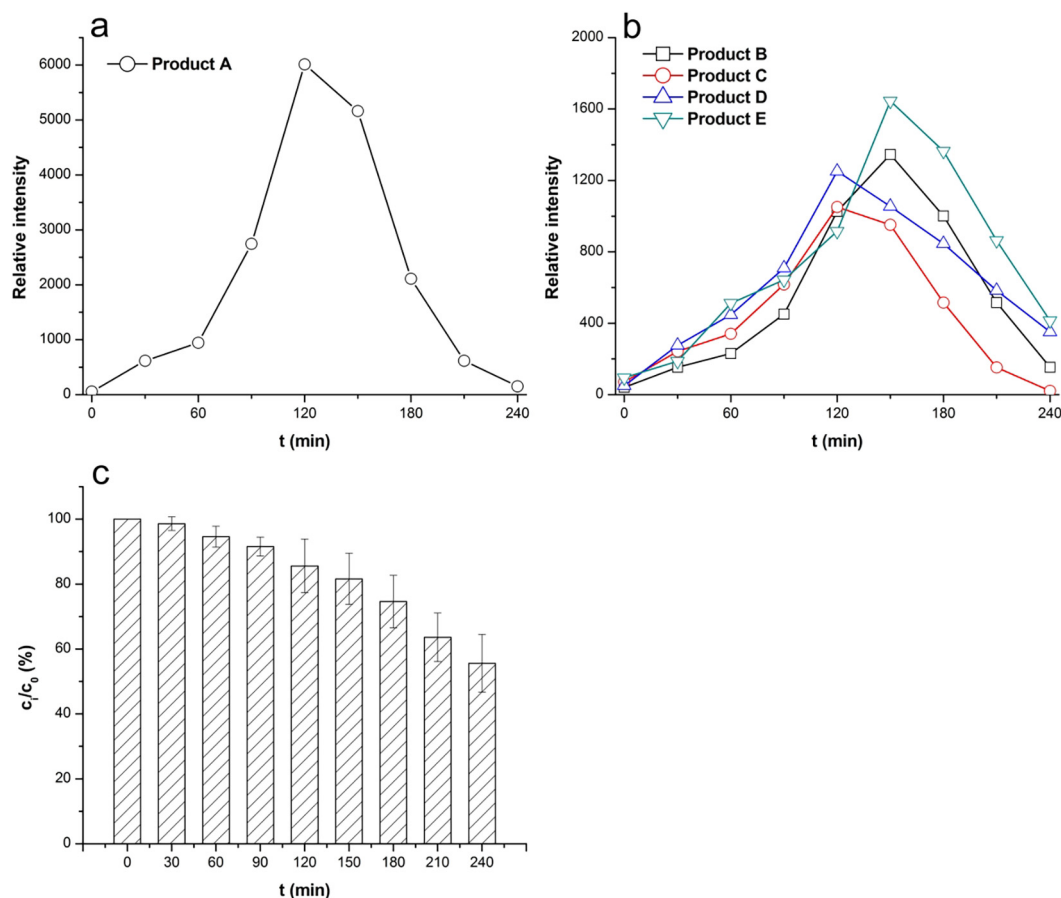


**Fig. 8.** Evolution curves of partial degradation products. (a) product A, (b) products B, C, D and E, (c) total organic matter. Experimental conditions: irradiation wavelength = 420 nm, irradiation intensity = 20.0 mW cm<sup>-2</sup>, [TCEP]<sub>0</sub> = 3.51 μM, [S<sub>2</sub>O<sub>8</sub><sup>2-</sup>]<sub>0</sub> = 500 mg L<sup>-1</sup>, [MIL-101(Fe)]<sub>m</sub> = 500 mg L<sup>-1</sup>, temperature = 298 K.

photocatalysts. A three times recycle was performed containing separation, washing, pre-adsorption and photocatalysis reactions. As shown in Fig. 6a, only a slight deactivation was observed. The final residual ratio of TCEP increased from 17% to 21%. The reduced removal efficiency can be explained by the slight metal-leaching of MIL-101(Fe). Of note, the two stages reaction still existed in recycled reactions as original reaction, suggesting that MIL-101(Fe) required a reactivation after drying.

Stability is also important for MOF. For Fe-based MOFs, leakage of Fe<sup>2+</sup> or Fe<sup>3+</sup> may also result in contamination of water matrixes, especially for drinking water treatment. In the current reaction system (pH = 3.00), 0.46 mg/L total iron ion was detected in the solution after 180-min reaction, while ~90% TCEP was removed. Generally, a good stability of MIL-101(Fe) was observed in acid condition. However, as pH value increased, a more serious iron release was observed. When pH increased to 11.00, the concentration of total iron increased to 13.9 mg L<sup>-1</sup> after 180 min reaction.

Based on Pearson's hard/soft acid/base principle, metal nodes and organic ligands in MOF can be considered as Lewis acid and Lewis bases, respectively. It was supposed that MOFs constructed by hard Lewis acid and hard Lewis bases can maintain its integrity under acid and neutral conditions, while combinations of soft Lewis acid and bases are stable in alkaline and neutral conditions [20]. Since the high-valent metal ions can be regarded as hard acids, while the carboxylate-based ligands can be regarded as hard bases, MIL-101(Fe) was supposed to be steady in acid and neutral conditions, but not in alkaline condition. This hypothesis was confirmed by the slight leakage of iron ion when pH = 3.00, which was aggravated when pH increased (Fig. 6b). The leaching of iron ion under acid condition may be due to the oxidation of the surface iron-benzoic acid complexes of MIL-101(Fe). In all, highest

degradation efficiency of TCEP was achieved under acid condition, with the lowest iron leaching (< 0.1% mass of adding MIL-101(Fe)).

### 3.8. Degradation products and pathways

To elucidate the degradation efficiency and mechanism in MOF/photo/persulfate system, determination of TCEP degradation products was performed. Based on the potential degradation reactions, several product candidates and their evaluation pathways were speculated (Fig. S3). After the HRMS analysis (Text S1), only five tentative candidates were confirmed (Fig. 7). Extracted ion chromatograms (EICs, retention time and *m/z* data) of these candidates are shown in Fig. S4, while the MS<sup>2</sup> chromatograms (fragment data) are shown in Fig. S5.

Structure verification of these product candidates was conducted based on MS<sup>2</sup> fragments. For example, product A (C<sub>4</sub>H<sub>9</sub>Cl<sub>2</sub>O<sub>4</sub>P, *m/z* 222.969 Da) had product ions at *m/z* 207.03, 191.00, 177.05, 172.86, 160.98, 149.02, 98.98, 63.00 Da (Fig. S6). The fragment ion peak at *m/z* 98.98 represented the phosphate backbone, while the difference between these product ions corresponded to the loss of fragments Cl (36 Da), CO (28 Da), H<sub>2</sub>O (18 Da), O (16 Da) and CH<sub>2</sub> (14 Da). Therefore, the structure of product A was elucidated, and the determination of other product candidates followed this similar procedure.

Relative intensity variation curves of these products are presented in Fig. 8. Product A reached the maximum value at ~120 min, while product B kept a high intensity at ~150 min, suggesting that products B was the further transformation product. Furthermore, maximum intensities of products C and D were observed at 120 min, while product E had a peak value at 150 min. According to their structure and intensity evolution results, the predominant pathway of TCEP in MOF/photo/persulfate system may involve cleavage, hydroxylation, carbonylation

and carboxylation. Of note,  $\cdot\text{SO}_4^-$  can react with  $\text{OH}^-$  to form  $\cdot\text{OH}$ . Since the pH value in product elucidation experiment was  $\sim 3.0$  (lack of  $\text{OH}^-$ ), low yield of  $\cdot\text{OH}$  implied  $\cdot\text{SO}_4^-$  based reactions would be dominant.  $\cdot\text{SO}_4^-$  is a nucleophile, the reaction mechanism would be mainly nucleophilic addition and substitution. The C=O bond in phosphorus backbone is relative stable, thus,  $\alpha$ -carbon adjacent to oxygen atom may be susceptible to  $\cdot\text{SO}_4^-$  attack. A cleavage of one oxygen-ethyl-chlorine arm occurred, resulting in generation of product A (Fig. 7b). Further cleavage will generate product B. The terminal C-Cl bonds are also susceptible to nucleophilic attack, resulting in a radical substitution to form product C (Fig. 7c). Theoretically, further oxidation products from products C, D and E would be generated (Fig. S3), which were reported in the existing study using UV/peroxymonosulfate for TCEP degradation [42]. However, no clear evidence about these further products was confirmed in the HRMS data here. This may be due to their low yields and concentrations in the current reaction. More generation steps a product required, lower probability a product occurred. TOC result is presented in Fig. 8c. TOC decreased as the reaction proceeded. After 240-min reaction, only 45% TOC was removed, implying an incomplete mineralization and residual of organic products. Even if the observed by-products were almost degraded, their further degradation products may still contain organic carbon structure.

#### 4. Conclusions

In this study, MIL-101(Fe) was prepared, and its performance as a photocatalyst in a MOF/photo/persulfate system for the degradation of TCEP was evaluated. Synthesized MIL-101(Fe) is regular crystal with high purity, and its light utilization highly depended on wavelength. Since it has an  $E_g$  at 2.41 eV, only irradiation  $< 520$  nm can activate the transformation of Fe(III) to Fe(II) in MIL-101(Fe), which induced further transformation of  $\text{S}_2\text{O}_8^{2-}$  into  $\cdot\text{SO}_4^-$ . Irradiation at 420 nm was confirmed to have the highest efficiency among all the visible light. Decreasing pattern of TCEP demonstrated a S-shape curve, including an induction period and a radical oxidation stage. Induction period would be a process involving adsorption of reactants and activating of MOF, while  $\cdot\text{SO}_4^-$  reactions was dominant in radical oxidation stage. Removal rates of these two stages highly depended on the reaction conditions. Acid condition (pH = 3.0), high temperature and high  $[\text{S}_2\text{O}_8^{2-}]$ : [MIL-101(Fe)] ratio were conducive. Five incomplete degradation products were elucidated, and the dominant degradation pathways included cleavage, hydroxylation, carbonylation and carboxylation. MIL-101(Fe) was stable in water matrixes under acid condition, and this MIL-101(Fe)/420 nm/persulfate system demonstrated a more robust performance than homogeneous UV/persulfate system for TCEP removal in real water matrixes, indicating that it is a potential technology for elimination of organic pollutants in water.

#### Acknowledgements

This project was supported by the National Natural Science Foundation of China (Grant No. 51778270) and the Fundamental Research Funds for the Central Universities (Grant Nos. 21617448, 17817020).

#### Appendix A. Supplementary data

Supplementary data to this article can be found online at <https://doi.org/10.1016/j.cej.2019.02.190>.

#### References

- [1] Y.L. Luo, W.S. Guo, H.H. Ngo, L.D. Nghiem, F.I. Hai, J. Zhang, S. Liang, X.C.C. Wang, A review on the occurrence of micropollutants in the aquatic environment and their fate and removal during wastewater treatment, *Sci. Total Environ.* 473 (2014) 619–641.
- [2] C.H. Wei, F.Z. Zhang, Y. Hu, C.H. Feng, H.Z. Wu, Ozonation in water treatment: the generation, basic properties of ozone and its practical application, *Rev. Chem. Eng.* 33 (2017) 49–89.
- [3] B.A. Wols, C.H.M. Hofman-Caris, Review of photochemical reaction constants of organic micropollutants required for UV advanced oxidation processes in water, *Water Res.* 46 (2012) 2815–2827.
- [4] S.O. Ganiyu, M.H. Zhou, C.A. Martinez-Huitle, Heterogeneous electro-Fenton and photoelectro-Fenton processes: a critical review of fundamental principles and application for water/wastewater treatment, *Appl. Catal. B-Environ.* 235 (2018) 103–129.
- [5] M.I. Stefan, *Advanced Oxidation Processes for Water Treatment: Fundamentals and Applications*, (2017) 9781780407197.
- [6] M. Gagol, A. Przyjazny, G. Boczkaj, Wastewater treatment by means of advanced oxidation processes based on cavitation – a review, *Chem. Eng. J.* 338 (2018) 599–627.
- [7] G. Boczkaj, A. Fernandes, Wastewater treatment by means of advanced oxidation processes at basic pH conditions: a review, *Chem. Eng. J.* 320 (2017) 608–633.
- [8] J.S. Ye, J. Liu, C.S. Li, P.L. Zhou, S. Wu, H.S. Ou, Heterogeneous photocatalysis of tris(2-chloroethyl) phosphate by UV/TiO<sub>2</sub>: degradation products and impacts on bacterial proteome, *Water Res.* 124 (2017) 29–38.
- [9] G.D. Fang, X.R. Chen, W.H. Wu, C. Liu, D.D. Dionysiou, T.T. Fan, Y.J. Wang, C.Y. Zhu, D.M. Zhou, Mechanisms of interaction between persulfate and soil constituents: activation, free radical formation, conversion, and identification, *Environ. Sci. Technol.* 52 (2018) 14352–14361.
- [10] Y. Zhou, X.L. Wang, C.Y. Zhu, D.D. Dionysiou, G.C. Zhao, G.D. Fang, D.M. Zhou, New insight into the mechanism of peroxymonosulfate activation by sulfur-containing minerals: role of sulfur conversion in sulfate radical generation, *Water Res.* 142 (2018) 208–216.
- [11] S.D. Hou, L. Ling, D.D. Dionysiou, Y.R. Wan, J.J. Huang, K.H. Guo, X.C. Li, J.Y. Fang, Chlorate formation mechanism in the presence of sulfate radical, chloride, bromide and natural organic matter, *Environ. Sci. Technol.* 52 (2018) 6317–6325.
- [12] S. Luo, Z.S. Wei, D.D. Dionysiou, R. Spinney, W.P. Hu, L.Y. Chai, Z.H. Yang, T.T. Ye, R.Y. Xiao, Mechanistic insight into reactivity of sulfate radical with aromatic contaminants through single-electron transfer pathway, *Chem. Eng. J.* 327 (2017) 1056–1065.
- [13] I.A. Ike, K.G. Linden, J.D. Orbell, M. Duke, Critical review of the science and sustainability of persulfate advanced oxidation processes, *Chem. Eng. J.* 338 (2018) 651–669.
- [14] Z.S. Wei, F.A. Villamena, L.K. Weavers, Kinetics and mechanism of ultrasonic activation of persulfate: an in situ EPR spin trapping study, *Environ. Sci. Technol.* 51 (2017) 3410–3417.
- [15] H.X. Liu, J.Y. Yao, L.H. Wang, X.H. Wang, R.J. Qu, Z.Y. Wang, Effective degradation of fenitrothion by zero-valent iron powder (Fe<sup>0</sup>) activated persulfate in aqueous solution: kinetic study and product identification, *Chem. Eng. J.* 358 (2019) 1479–1488.
- [16] M. Usman, P. Faure, C. Ruby, K. Hanna, Application of magnetite-activated persulfate oxidation for the degradation of PAHs in contaminated soils, *Chemosphere* 87 (2012) 234–240.
- [17] D.H. Ding, C. Liu, Y.F. Ji, Q. Yang, L.L. Chen, C.L. Jiang, T.M. Cai, Mechanism insight of degradation of norfloxacin by magnetite nanoparticles activated persulfate: identification of radicals and degradation pathway, *Chem. Eng. J.* 308 (2017) 330–339.
- [18] C.J. Liang, C.J. Bruell, M.C. Marley, K.L. Sperry, Persulfate oxidation for in situ remediation of TCE. I. Activated by ferrous ion with and without a persulfate-thiosulfate redox couple, *Chemosphere* 55 (2004) 1213–1223.
- [19] M. Feng, P. Zhang, H.-C. Zhou, V.K. Sharma, Water-stable metal-organic frameworks for aqueous removal of heavy metals and radionuclides: a review, *Chemosphere* 209 (2018) 783–800.
- [20] S. Yuan, L. Feng, K. Wang, J. Pang, M. Bosch, C. Lollar, Y. Sun, J. Qin, X. Yang, P. Zhang, Q. Wang, L. Zou, Y. Zhang, L. Zhang, Y. Fang, J. Li, H.-C. Zhou, Stable metal-organic frameworks: design, synthesis, and applications, *Adv. Mater.* (Deerfield Beach, Fla.) (2018).
- [21] H.L. Lv, H.Y. Zhao, T.C. Cao, L. Qian, Y.B. Wang, G.H. Zhao, Efficient degradation of high concentration azo-dye wastewater by heterogeneous Fenton process with iron-based metal-organic framework, *J. Mole. Catal. A-Chem.* 400 (2015) 81–89.
- [22] C. Gao, S. Chen, X. Quan, H.T. Yu, Y.B. Zhang, Enhanced Fenton-like catalysis by iron-based metal organic frameworks for degradation of organic pollutants, *J. Catal.* 356 (2017) 125–132.
- [23] Y. Gao, S. Li, Y. Li, L. Yao, H. Zhang, Accelerated photocatalytic degradation of organic pollutant over metal-organic framework MIL-53(Fe) under visible LED light mediated by persulfate, *Appl. Catal. B-Environ.* 202 (2017) 165–174.
- [24] J.T. Tang, J.L. Wang, Fe-based metal organic framework/graphene oxide composite as an efficient catalyst for Fenton-like degradation of methyl orange, *RSC Adv.* 7 (2017) 50829–50837.
- [25] M.-J. Duan, Z.-Y. Guan, Y.-W. Ma, J.-Q. Wan, Y. Wang, Y.-F. Qu, A novel catalyst of MIL-101(Fe) doped with Co and Cu as persulfate activator: synthesis, characterization, and catalytic performance, *Chem. Pap.* 72 (2018) 235–250.
- [26] X.W. Feng, H. Cheri, F. Jiang, In-situ ethylenediamine-assisted synthesis of a magnetic iron-based metal-organic framework MIL-53(Fe) for visible light photocatalysis, *J. Colloid Interface Sci.* 494 (2017) 32–37.
- [27] K.Y.A. Lin, F.K. Hsu, Magnetic iron/carbon nanorods derived from a metal organic framework as an efficient heterogeneous catalyst for the chemical oxidation process in water, *RSC Adv.* 5 (2015) 50790–50800.
- [28] S.X. Li, S.L. Sun, H.Z. Wu, C.H. Wei, Y. Hu, Effects of electron-donating groups on the photocatalytic reaction of MOFs, *Catal. Sci. Technol.* 8 (2018) 1696–1703.

- [29] E.L. Schymanski, J. Jeon, R. Gulde, K. Fenner, M. Ruff, H.P. Singer, J. Hollender, Identifying small molecules via high resolution mass spectrometry: communicating confidence, *Environ. Sci. Technol.* 48 (2014) 2097–2098.
- [30] D.B. Wang, F.Y. Jia, H. Wang, F. Chen, Y. Fang, W.B. Dong, G.M. Zeng, X.M. Li, Q. Yang, X.Z. Yuan, Simultaneously efficient adsorption and photocatalytic degradation of tetracycline by Fe-based MOFs, *J. Colloid Interface Sci.* 519 (2018) 273–284.
- [31] X. Li, W. Guo, Z. Liu, R. Wang, H. Liu, Quinone-modified NH<sub>2</sub>-MIL-101(Fe) composite as a redox mediator for improved degradation of bisphenol A, *J. Hazard. Mater.* 324 (2017) 665–672.
- [32] C.C. Zhao, P. Dong, Z.M. Liu, G.R. Wu, S.J. Wang, Y.Q. Wang, F. Liu, Facile synthesis of Fe<sub>3</sub>O<sub>4</sub>/MIL-101 nanocomposite as an efficient heterogeneous catalyst for degradation of pollutants in Fenton-like system, *RSC Adv.* 7 (2017) 24453–24461.
- [33] X. Li, W. Guo, Z. Liu, R. Wang, H. Liu, Fe-based MOFs for efficient adsorption and degradation of acid orange 7 in aqueous solution via persulfate activation, *Appl. Surf. Sci.* 369 (2016) 130–136.
- [34] R. Lopez, R. Gomez, Band-gap energy estimation from diffuse reflectance measurements on sol-gel and commercial TiO<sub>2</sub>: a comparative study, *J. Sol-Gel Sci. Technol.* 61 (2012) 1–7.
- [35] H.-S. Ou, J. Liu, J.-S. Ye, L.-L. Wang, N.-Y. Gao, J. Ke, Degradation of tris(2-chloroethyl) phosphate by ultraviolet-persulfate: kinetics, pathway and intermediate impact on proteome of *Escherichia coli*, *Chem. Eng. J.* 308 (2017) 386–395.
- [36] J.G. Carriazo, E. Guelou, J. Barrault, J.M. Tatibouet, S. Moreno, Catalytic wet peroxide oxidation of phenol over Al-Cu or Al-Fe modified clays, *Appl. Clay Sci.* 22 (2003) 303–308.
- [37] M.L. Luo, D. Bowden, P. Brimblecombe, Catalytic property of Fe-Al pillared clay for Fenton oxidation of phenol by H<sub>2</sub>O<sub>2</sub>, *Appl. Catal. B-Environ.* 85 (2009) 201–206.
- [38] C. Park, R.T.K. Baker, Modifications in the catalytic properties of nickel supported on different dielectric oxides, *Chem. Mater.* 14 (2002) 273–280.
- [39] A. Ghauch, A.M. Tuqan, N. Kibbi, Ibuprofen removal by heated persulfate in aqueous solution: a kinetics study, *Chem. Eng. J.* 197 (2012) 483–492.
- [40] O.S. Furman, A.L. Teel, R.J. Watts, Mechanism of base activation of persulfate, *Environ. Sci. Technol.* 44 (2010) 6423–6428.
- [41] J. Liu, J.S. Ye, Y.F. Chen, C.S. Li, H.S. Ou, UV-driven hydroxyl radical oxidation of tris(2-chloroethyl) phosphate: intermediate products and residual toxicity, *Chemosphere* 190 (2018) 225–233.
- [42] X.X. Xu, J. Chen, R.J. Qu, Z.Y. Wang, Oxidation of Tris (2-chloroethyl) phosphate in aqueous solution by UV-activated peroxymonosulfate: kinetics, water matrix effects, degradation products and reaction pathways, *Chemosphere* 185 (2017) 833–843.